

Highly nondegenerate femtosecond four-wave mixing in tapered microstructure fiber

Kazi S. Abedin, Juliet T. Gopinath, Erich P. Ippen, Charles E. Kerbage, Robert S. Windeler, and Benjamin J. Eggleton

Citation: [Applied Physics Letters](#) **81**, 1384 (2002); doi: 10.1063/1.1501440

View online: <http://dx.doi.org/10.1063/1.1501440>

View Table of Contents: <http://scitation.aip.org/content/aip/journal/apl/81/8?ver=pdfcov>

Published by the [AIP Publishing](#)

Articles you may be interested in

[Strong field effects in rotational femtosecond degenerate four-wave mixing](#)

J. Chem. Phys. **132**, 134301 (2010); 10.1063/1.3367726

[Single-walled carbon-nanotube-deposited tapered fiber for four-wave mixing based wavelength conversion](#)

Appl. Phys. Lett. **96**, 061104 (2010); 10.1063/1.3304789

[Intermodal four-wave mixing from femtosecond pulse-pumped photonic crystal fiber](#)

Appl. Phys. Lett. **94**, 101109 (2009); 10.1063/1.3094127

[Femtosecond degenerate four-wave mixing of carbon disulfide: High-accuracy rotational constants](#)

J. Chem. Phys. **124**, 144307 (2006); 10.1063/1.2186642

[Nondegenerate four-wave mixing in a semiconductor microcavity](#)

Appl. Phys. Lett. **71**, 2650 (1997); 10.1063/1.120168



AIP | Journal of
Applied Physics

Journal of Applied Physics is pleased to
announce **André Anders** as its new Editor-in-Chief

Highly nondegenerate femtosecond four-wave mixing in tapered microstructure fiber

Kazi S. Abedin,^{a)} Juliet T. Gopinath,^{b)} and Erich P. Ippen^{c)}

Department of Electrical Engineering and Computer Science, Research Laboratory of Electronics, Massachusetts Institute of Technology, Cambridge, Massachusetts 02139

Charles E. Kerbage, Robert S. Windeler, and Benjamin J. Eggleton^{d)}

OFS Laboratories, Murray Hill, New Jersey 07974

(Received 9 April 2002; accepted for publication 25 June 2002)

We demonstrate efficient, highly nondegenerate four-wave mixing of femtosecond pulses, with a frequency shift of $\sim 6000\text{ cm}^{-1}$, in an 18 cm tapered microstructure fiber. Using a pump at 810 nm and a signal at 1540 nm, light is generated at wavelengths between 535 nm and 570 nm with 10% efficiency. Due to the walk-off between pump and signal pulses in the fiber, the interaction length in the tapered fiber is only 1.4 cm. Ten percent efficiency is achieved in this short length because of the enhanced nonlinearity of the tapered fiber and its unique dispersion characteristics. © 2002 American Institute of Physics. [DOI: 10.1063/1.1501440]

Four-wave mixing (FWM) is a useful technique for wavelength conversion,^{1,2} phase conjugation,³ squeezing,⁴ and frequency metrology.⁵ It has been demonstrated in gases, semiconductors, crystals, and optical fibers. Optical fibers are attractive because of their large bandwidth, low loss, and long interaction lengths. In 1974, FWM with a frequency shift of 2800 cm^{-1} was observed in a 9 cm $\text{SiO}_2:\text{B}_2\text{O}_3$ clad waveguide, with a peak pump power of 100 W.⁶ In 1981, with 25 kW of peak power, a frequency shift of 2900 cm^{-1} was observed in 1 m of graded index multimode fiber.⁷ Recently, a frequency shift of 100 cm^{-1} was observed in 6.1 m of microstructure fiber, which had a small core ($1.7\text{ }\mu\text{m}$) for nonlinear enhancement.⁸ The FWM technique has also been used for converting femtosecond pulses at 1.5 to $1.3\text{ }\mu\text{m}$.⁹ However, material and waveguide dispersion, which contribute to phase mismatch and group velocity differences, have made it difficult to achieve highly nondegenerate FWM with femtosecond pulses. The advent of fiber with “engineered” dispersion and nonlinearity profiles has mitigated these problems.

In this letter, we demonstrate highly nondegenerate FWM with frequency shifts as large as 6000 cm^{-1} . This is achieved with femtosecond pulses at 1540 and 810 nm in a tapered air-silica microstructure fiber (T-ASMF).¹⁰ The idler (FWM) wave is generated at wavelengths ranging from 537 to 575 nm, with a maximum conversion efficiency of 10% in an interaction length of 1.4 cm. Highly nondegenerate four-wave mixing is possible because of the kW peak powers of the femtosecond pulses, the dispersion profile of the fiber, and the high nonlinearity of the fiber.

The tapering of the microstructure fiber produces a small core diameter of $\sim 3\text{ }\mu\text{m}$, enhancing the nonlinearity by an order of magnitude.¹⁰ The presence of air holes in the cladding results in a large core-clad index difference of ~ 0.3 .

With this large index difference and small core size, the T-ASMF can compensate material dispersion and allow phase matching between highly nondegenerate waves in the lowest order mode. In addition to FWM, third-harmonic generation (THG) from the 1540 nm light is observed. If an octave-spanning spectra is launched into the fiber, interference between FWM and THG could provide a simple method for frequency referencing.⁵

The experimental setup is shown in Fig. 1. Pulses from a femtosecond optical parametric oscillator (1540 nm), the signal, and from a Ti:Sapphire laser (810 nm), the pump, were launched into an 18 cm T-ASMF fiber section with a core diameter of $3\text{ }\mu\text{m}$ (outer diameter: $10\text{ }\mu\text{m}$). Before tapering, the fiber (ASMF) consists of a $\sim 8\text{-}\mu\text{m}$ -diameter Ge-doped core, surrounded with a $\sim 40\text{ }\mu\text{m}$ silica region. An outer cladding ($132\text{ }\mu\text{m}$ diameter) surrounds this. In this outer cladding, there is a hexagonal ring of six ($\sim 30\text{ }\mu\text{m}$ diameter) air holes. The T-ASMF section was formed by adiabatic tapering¹⁰ of the ASMF from an outer diameter of 132 to $10\text{ }\mu\text{m}$, as shown in Fig. 1. As fiber is tapered, light can no longer be confined by the core, but instead propagates through the central silica region (which is about $3\text{ }\mu\text{m}$ in the taper), confined by the air holes. After the tapering, the Ge in the initially doped core is diffused throughout the entire central silica region of the microstructure fiber.

To adjust the relative timing of the signal and pump pulses, a variable time delay was placed in the path of the

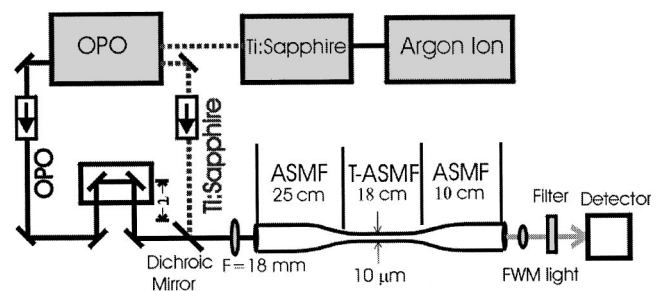


FIG. 1. Experimental setup for highly nondegenerate FWM.

^{a)}Presently with: Communications Research Laboratory, Tokyo, Japan.

^{b)}Electronic mail: juliet@mit.edu

^{c)}Also with: the Department of Physics.

^{d)}Also with: OFS Specialty Photonics Division, Somerset, New Jersey.

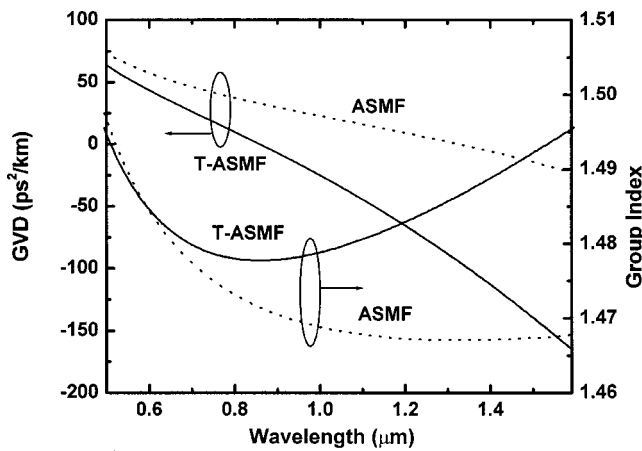


FIG. 2. Calculated group index and GVD vs wavelength for the ASMF and T-ASMF.

signal wave. The beams were combined using a dichroic mirror and launched into the ASMF with an aspheric lens ($f=18$ mm). Coupling efficiencies into the fiber for the signal and pump ranged from 30% to 40%. The relatively low air-to-fiber coupling efficiency was due to the differing spot sizes for the two wavelengths, and the wavelength dependency of the lens focal length and antireflection coating. At the other end of the ASMF, the FWM wave was focused onto a silicon photodetector. Before reaching the T-ASMF, the pulses propagate through an ASMF region. Simulations show that the pump pulses, initially ~ 190 fs (full width at half maximum), broaden to ~ 620 fs in the ASMF. The signal pulses, 150 fs to start, are actually compressed to ~ 100 fs.

Due to the large wavelength separation, the pump and the signal pulses walk-off from each other as they propagate through the T-ASMF fiber. The interaction length can be determined from the group index, n_g . We performed numerical simulations to determine n_g and the group velocity dispersion (GVD) of the T-ASMF. We assumed a step-index fiber, with a core-clad index difference of 0.3 and a core diameter of $3 \mu\text{m}$. The material dispersion in the T-ASMF is calculated using the Sellmeier equation of bulk silica.¹¹ The solid lines in Fig. 2 show the calculated values of group index and GVD versus wavelength for the lowest order HE mode in the T-ASMF. The dotted lines in Fig. 2 show the group index and GVD for the ASMF ($8 \mu\text{m}$ core). These are calculated for the lowest order HE mode in the ASMF, using parameters for Ge-doped silica. We obtain a group index difference of 0.0157 for the lowest order HE mode in the T-ASMF, giving an interaction length of 1.4 cm. The zero dispersion wavelength was estimated to be ~ 858 nm.

When the pump pulse is launched alone, self-phase modulation causes the 10 nm spectrum to broaden to 55 nm. When the signal is added, we observed idler with wavelengths ranging from 537 to 575 nm. A typical optical spectrum of the idler wave is shown in Fig. 3. In Fig. 4, the idler power is plotted as a function of the incident pump power, with constant signal power. The parabolic dependence indicates that two photons of Ti Sapphire beam are annihilated to generate one photon of idler through the FWM process.

With a maximum incident pump power of 180 mW and signal power of 80 mW, we were able to generate ~ 4 mW of idler light from the fiber. The coupling efficiency of the

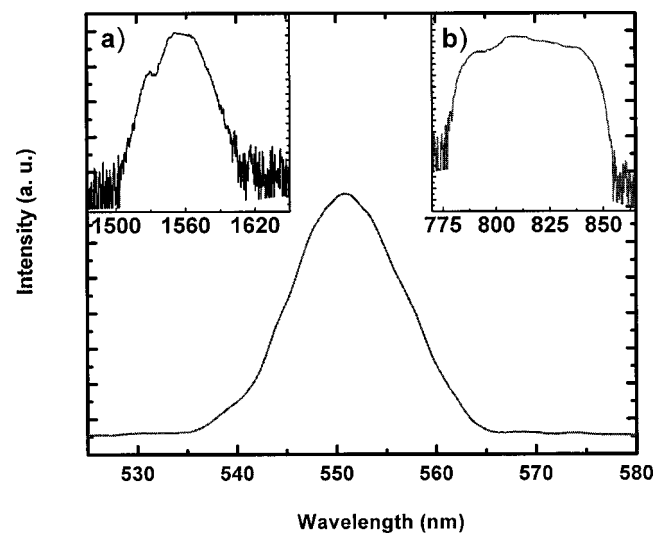


FIG. 3. Spectrum of idler (linear scale). Insets: (a) signal spectrum (log scale), (b) pump spectrum (log scale).

pump beam was 33% and that of the signal, 44%. The efficiency of the FWM process, defined as $P_{\text{idler}}/P_{\text{signal}}$, was $\sim 10\%$ (-10 dB). The green output power is $\sim 9\%$ of the maximum power obtainable, calculated from the Manly-Rowe relations of photon conservation. It is possible that the idler does not remain in the lowest order mode and is instead converted to higher order modes, degrading the efficiency.

We derived an expression for the parametric gain coefficient of highly nondegenerate FWM following the approaches of Refs. 1, 12 and 13. We assumed an undepleted pump, a weak signal, a constant value for the nonlinear refractive index n_2 , a single effective overlap integral, and no loss. We obtained

$$g = \sqrt{(\gamma_{\text{eff}} P_p)^2 - (\kappa/2)^2}, \quad (1)$$

where $\gamma_{\text{eff}} = (2\pi/\sqrt{\lambda_i \lambda_s})(n_2/A_{\text{eff}})$; λ_s is the signal wavelength; λ_i , the idler wavelength; A_{eff} , the effective mode area; and P_p , the peak pump power. The parameter κ is the phase mismatch,

$$\kappa = \Delta k + 2\gamma_p P_p. \quad (2)$$

Here, the term $2\gamma_p P_p$ is the induced pump nonlinearity with $\gamma_p = (2\pi/\lambda_p)(n_2/A_{\text{eff}})$. The wave vector mismatch

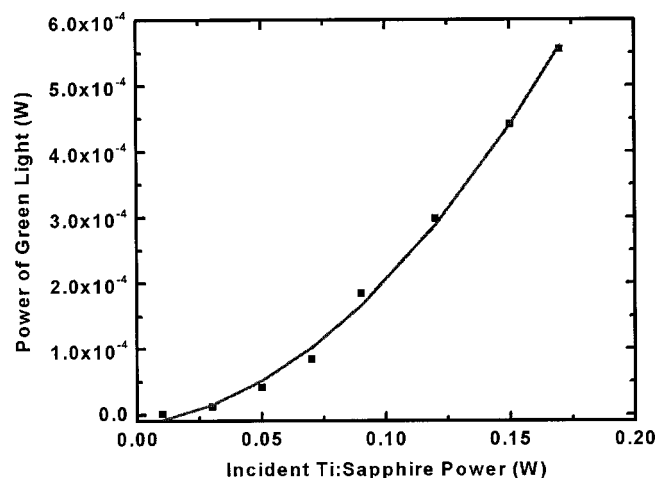


FIG. 4. Power dependence of the idler on incident pump.

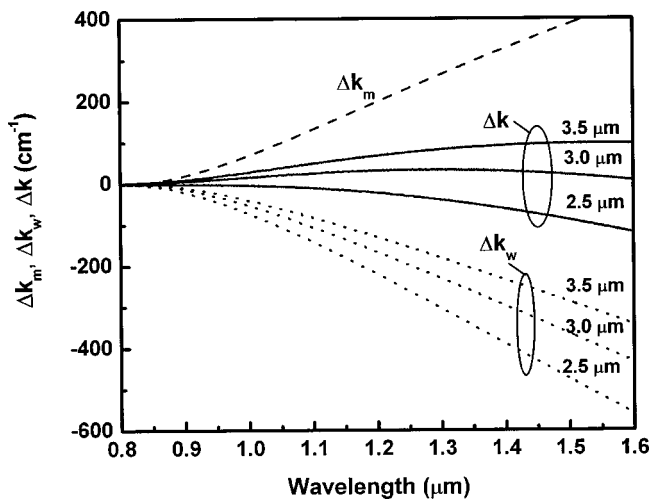


FIG. 5. Calculated wavevector mismatch vs signal wavelength (pump wavelength constant, 810 nm) for T-ASMF with core diameters of 2.5, 3.0, and 3.5 μm . Pump, signal, and idler are in the HE_{11} mode. The core-clad index difference is assumed constant (0.3). Δk_m : material contribution; Δk_w : waveguide contribution; Δk : sum.

between the signal, idler, and pump, Δk , is defined as $\Delta k = k_s + k_i - 2k_p$. In an optical fiber, Δk results from the bulk medium (Δk_m) and the waveguide (Δk_w). For a pump at 810 nm and signal at 1540 nm. Δk_m in fused silica can be as large as 408 cm^{-1} . This large wave vector mismatch cannot be compensated with the waveguide contribution in conventional fibers, which have a core-clad index difference of ~ 0.005 . However, the T-ASMF fiber, with an index difference of 0.3, gives a waveguide contribution comparable to the material contribution. Figure 5 plots the wavevector phase mismatch terms Δk_m , Δk_w , and their sum, versus signal wavelength (constant pump wavelength). These values are plotted for core diameters of 2.5, 3.0, and 3.5 μm . The curves are calculated using a vectorial analysis of a step index fiber with an index difference of 0.3, and with all waves in the lowest order mode, HE_{11} . It is clear that the material contribution Δk_m can be compensated by the waveguide contribution Δk_w , for T-ASMF fibers with diameters of $\sim 3 \mu\text{m}$ and core-clad index differences of 0.3. A more accurate determination of the optimum core size should take into account the weak dependence of the effective index difference on the wavelength.¹⁴ Higher order modes of the pump may also be excited, but their phase velocities do not allow phase matching. Since Δk depends strongly on the core diameter, it is difficult to precisely determine the coherence length l_{coh} for the T-ASMF. Using the curves in Fig. 5, we calculated the value of l_{coh} as .06, 0.44, and .06 cm for core diameters 2.5, 3.0, and 3.5 μm , respectively.

We calculated an upper bound for the maximum conversion efficiency with the formula,

$\eta = (\lambda_s/\lambda_i)(\gamma_{\text{eff}}P_p/g)^2 \sinh^2(gL)$. This assumes an undepleted pump, a weak signal, a constant value for nonlinearity (n_2), a single effective overlap integral, and no loss.^{1,13} Using $P_p = 1168 \text{ W}$, $n_2 = 3.2 \times 10^{-20} \text{ m}^2/\text{W}$, $A_{\text{eff}} = 5 \mu\text{m}^2$, $L = 1.4 \text{ cm}$, and $\kappa = 0$, we calculate a maximum conversion efficiency of 168%. Note that the conversion efficiency, defined as $P_{\text{idler}}/P_{\text{signal}}$, can easily exceed 100%. The discrepancy between the experiment and theory results from deviations in phase matching, uncertainty in the value of mode overlap integrals and in the value of n_2 , and loss due to higher-order mode coupling and scattering. Further enhancements in conversion efficiency are expected through fine adjustment of the core diameter of the T-ASMF.

In conclusion, we have demonstrated highly nondegenerate FWM with frequency shifts as large as 6000 cm^{-1} in T-ASMF fiber. A conversion efficiency of 10% was obtained in an interaction length of only 1.4 cm. This was possible because of the enhanced nonlinearity of the T-ASMF, the unique dispersion profile of the T-ASMF, and the high peak power of the femtosecond pulses used. Similar interactions in such fibers could be used for applications in squeezing, frequency metrology, and wavelength conversion.

We gratefully acknowledge helpful discussions with P. Rakich and A. Gopinath. One author (K.S.A.) acknowledges support from the Japanese Science and Technology Agency. This project was sponsored in part by AFOSR and DARPA.

- ¹G. P. Agrawal, *Nonlinear Fiber Optics* (Academic, San Diego, 1986).
- ²C. Dorman, I. Kucukkara, and J. P. Marangos, *Phys. Rev. A* **61**, 013802 (1999).
- ³R. W. Hellwarth, *J. Opt. Soc. Am. B* **67**, 1 (1977).
- ⁴R. E. Slusher, L. W. Hollberg, B. Yurke, J. C. Mertz, and J. F. Valley, *Phys. Rev. Lett.* **55**, 2409 (1985); M. D. Levenson, R. M. Shelby, and S. H. Perlmutter, *Opt. Lett.* **10**, 514 (1985).
- ⁵S. A. Diddams, D. J. Jones, J. Ye, S. T. Cundiff, J. L. Hall, J. K. Ranka, and R. S. Windeler, *IEEE Trans. Instrum. Meas.* **50**, 552 (2001).
- ⁶R. H. Stolen, J. E. Bjorkholm, and A. Ashkin, *Appl. Phys. Lett.* **24**, 308 (1974).
- ⁷K. O. Hill, D. C. Johnson, and B. S. Kawasaki, *Appl. Opt.* **20**, 1075 (1981).
- ⁸J. E. Sharping, M. Fiorentino, A. Coker, P. Kumar, and R. S. Windeler, *Opt. Lett.* **26**, 1048 (2001).
- ⁹Z. Su, X. Zhu, and W. Sibbett, *J. Opt. Soc. Am. B* **10**, 1050 (1993).
- ¹⁰X. Liu, C. Xu, W. H. Knox, J. K. Chandalia, B. J. Eggleton, S. G. Kosinski, and R. S. Windeler, *Opt. Lett.* **26**, 358 (2001); B. J. Eggleton, C. Kerbage, P. Westbrook, R. S. Windeler, and A. Hale, *Opt. Express* **9**, 698 (2001).
- ¹¹A. Ghatak and K. Thyagarajan, *Introduction to Fiber Optics* (Cambridge University Press, Cambridge, 1998).
- ¹²R. H. Stolen and J. E. Bjorkholm, *IEEE J. Quantum Electron.* **18**, 1062 (1982).
- ¹³G. A. Nowak, Y.-H. Kao, T. J. Xia, and M. N. Islam, *Opt. Lett.* **23**, 936 (1998).
- ¹⁴A. Ferrando, E. Silvestre, J. J. Miret, and P. Andres, *Opt. Lett.* **25**, 790 (2000).